Journal of Chromatography, 503 (1990) 127–154
Elsevier Science Publishers B.V., Amsterdam — Printed in The Netherlands

CHROM 22 170

Evaluation of refractive index artifacts in liquid chromatographic absorbance detection

Extension to non-ideal injection and gradient elution

CHRISTINE E. EVANS and VICTORIA L. McGUFFIN*
Department of Chemistry, Michigan State University, East Lansing, MI 48824 (U.S.A.)
(First received June 21st, 1989; revised manuscript received November 23rd, 1989)

SUMMARY

An anomalous response is often observed in high-sensitivity absorbance detection upon a rapid change in solvent composition. This detector artifact appears to be related to refractive index gradients arising when the injection solvent differs from the mobile phase or during solvent programming. Because this anomalous response is often of the same magnitude as the true solute absorbance, misinterpretation of the acquired chromatogram may result. Characterization of this refractive index artifact has been accomplished by modelling the Z-pattern flow cell as a dynamic lens, with constantly changing refractive index profiles both radial and axial to the direction of flow. A ray-tracing algorithm is utilized to predict the final image diameter and the apparent absorbance caused by the changing refractive index conditions. Initial predictions for an ideal, delta function injection show excellent correlation with the experimentally observed response for a commercially available absorbance detector. Simulations are extended to include the more complex axial profiles commonly encountered in liquid chromatography, including those arising from non-ideal injection conditions as well as solvent programming. Predictions based on this model show good agreement with the shape, direction and magnitude of the observed detector response. In addition to aiding in the characterization of solute peaks, this ray-tracing model has direct implications for the accurate interpretation of system peaks in liquid chromatography. Although investigations described here are limited to the Z-pattern cell, this dynamic lens model may be adapted to the evaluation or improved design of any flow cell of interest.

INTRODUCTION

Absorbance detectors utilized in liquid chromatography often exhibit an anomalous response upon a rapid change in solvent composition. These artifacts appear to be related to gradients in refractive index created when the concentration is varied abruptly, as might occur upon injection or solvent programming[1]. Although the

0021-9673/90/$03.50

exact origin of this anomaly is not clear, rapid changes in solvent composition, and thus refractive index, apparently create a "dynamic lens" inside the flow cell. As qualitatively described by Betteridge *et al.*[2], the continually changing refractive index conditions cause incident light to be refracted toward and away from the photodiode transducer, resulting in a detector response even though no absorbing species are present. More recently, Hancock and Synovec[3] cite an interferometric mechanism as the origin of this anomalous response. Unfortunately, only a few published studies have attempted to address the origin and nature of this anomaly.

Previous investigations of the refractive index artifact have focussed on the elimination of this deleterious effect in absorbance detection. To minimize the refractive index dependence, modifications in both external optics and cell design have been proposed for the most common flow cell configuration, the Z-pattern cell. The role of external optics has been investigated by Stewart for static[4] as well as dynamic[5] refractive index conditions. In both cases, optical calculations indicate the necessity of focussing incident radiation near the flow cell exit to allow all light to pass through the cell under all refractive index conditions. When incident light is focussed in this manner, the throughput is no longer limited by the flow cell exit aperture, and thus, the dependence of detector response on refractive index is minimized. Implementation of this external optical arrangement has proven difficult due to chromatographic requirements for small detector cell volumes. For example, this optical design would require that incident radiation from an extended source be focussed at the exit of a cell less than 0.5 mm diameter and 1 cm long. Although focussing the incident light in this manner is feasible[6], such external optics become difficult if a rugged detection system with interchangeable cell options is desired. Alternatively, the flow cell body can be redesigned as proposed by Little and Fallick[7]. In their design, the cell exit aperture is larger than the entrance aperture, thus allowing all incident light to pass through the cell regardless of solvent refraction. Unfortunately, the change in radius within the flow cell often results in an increase in cell volume and may complicate flow dynamics, leading to additional band broadening. For these reasons, the above modifications have not been implemented in many commercially available absorbance detectors.

Although the refractive index artifact is often detrimental in absorbance detection, it can be utilized to advantage in the design of refractive index detectors for both flow injection analysis and liquid chromatography. Betteridge *et al.*[2] couple a light-emitting diode source (λ = 565 nm) and photodiode detector together with a 95-μl U-pattern flow cell for the detection of various salt solutions injected into a flowing stream of water. The detector response, similar in shape to the first derivative of a Gaussian function, is observed with detection limits of approximately $1 \cdot 10^{-3}$ *M* (0.1%) sodium chloride. Bornhop *et al.*[8] also utilize this refractive index response in a simple capillary flow cell design by focussing a helium–neon laser (λ = 633 nm) slightly off-center and perpendicular to the cell. In this case, refraction of the incident light produces an interference pattern. A small-area photodiode is then utilized to monitor the movement of the interference fringes induced by the changing refractive index conditions within the cell. Detection limits of $3 \cdot 10^{-6}$ *M* (0.9 ppm) are shown for sucrose in a separation of simple sugars. Pawliszyn[9] describes a fiber optic detector design as being sensitive to refractive index, and hence, to concentration gradients within the flow cell. The detected signal is evaluated based on Schlieren optics and is measured as a change in the deflection angle utilizing a position-sensitive

photodiode. A sheath flow cell is used to enhance the detector response resulting in a detection limit of approximately $5 \cdot 10^{-6}$ M (2 ppm) sucrose[10]. Recently, Hancock and Synovec[3] have utilized a Z-pattern cell design for the refractive index detection of polymers in size-exclusion chromatography, with detection limits of $2 \cdot 10^{-9}$ M (0.9 ppm) polystyrene. Although many of these detector designs provide a simple and rugged means for solute detection, the exact nature of the detected signal has not yet been fully described in the literature. Ultimately, optimization of these designs requires a more detailed understanding of the refractive index artifacts responsible for the detector response.

In this study, theoretical predictions and experimental observations are combined in an effort to understand more clearly the nature of the refractive index artifact. Theoretical evaluation of the detector response is accomplished by modelling the flow cell as a dynamic lens. By incorporating refractive index gradients both radial and axial to the direction of flow, this ray-tracing model allows a more systematic evaluation of the possible origin(s) of the detector response. Preliminary simulations employing this model predict the detector response for a Z-pattern flow cell utilizing a parabolic radial refractive index gradient, characteristic of laminar flow[11]. These initial predictions for an ideal Gaussian axial gradient confirm the derivative-shaped response commonly observed upon injection. Simulation results indicate that both the radial and axial components of the refractive index gradient are necessary to predict the detector response accurately. Although these preliminary simulations describe only ideal gradients, the model shows excellent agreement with the experimental measurement of both the final image size and intensity[11]. Unfortunately, many gradients commonly encountered in liquid chromatography may not be ideal. In the present work, characterization of the refractive index artifact for non-ideal axial gradients is accomplished by correlating predicted detector response with experimental observations. By extending these studies to include complex axial gradients occurring upon injection or solvent programming, the validity of the "dynamic lens" model can be more rigorously tested under practical experimental conditions.

THEORY

The transmittance of electromagnetic radiation in any optical system can be described as the ratio of the light intensity transmitted (I) to that incident (I_0) on the flow cell. This concept forms the basis for absorbance detection in liquid chromatography, where the transmittance ($T = I/I_0$) is altered by any species which absorbs radiation at a given wavelength. It is assumed that the detector response is directly proportional to the concentration of absorbing species in the flow cell as a function of time. However, as with any optical system, the refractive index of the material present in the flow cell can also affect the system transmittance, and thus the apparent absorbance. Unlike deviations in Beer's law resulting from anomalous dispersion or changes in viewed volume[12], this refractive index artifact occurs even when no absorbing species are present.

With no absorbers within the flow cell, the system transmittance is a function of both the field stop and the aperture stop. Because the field stop restricts the field of view of the optical system and the aperture stop limits the amount of light reaching the detector, both must be considered when calculating the system transmittance. This

determination can be accomplished from the product of the field stop area and the solid angle subtended by the aperture stop[13]. Direct determination of the solid angle is possible by tracing the outermost incident ray which is transmitted through the optical system. By evaluating the angle of light deflection at each interface with the familiar Snell's law expression, the maximum incident angle limited by the aperture stop, and thus the system transmittance, can be determined. Since both optical stops are located at or within the flow cell for many absorbance detector designs, such calculations require information about light incident on the flow cell as well as refractive index conditions within the cell.

Although a variety of incident light conditions are possible, many optical designs for the common Z-pattern flow cell utilize the entrance aperture of the cell as the exit slit of the monochromator. In this case, the flow cell entrance aperture is overfilled and forms the field stop in the optical system, thereby restricting the field of view. The cell exit aperture can then act as the system aperture stop, limiting the amount of light reaching the detector. Thus, the flow cell transmittance can be calculated directly from the area of the cell entrance aperture and solid angle restricted by the cell exit aperture.

Calculation of the cell entrance area is trivial, but calculation of the solid angle requires knowledge of the refractive index conditions. For a static system, the refractive index of the solvent within the flow cell is known and thus, the transmittance may be calculated directly[4]. This is, however, not true in a dynamic chromatographic system, where the solution refractive index in the cell may be continually changing with time. Moreover, refractive index gradients arising within the flow cell itself due to flow pattern and mixing further complicate the transmittance calculation. Thus, to evaluate the transmittance under flow conditions, characterization of the refractive index profiles in the cell volume is necessary.

In a dynamic system, refractive index profiles exist within the flow cell both radial [$n(r)$] and axial [$n(z)$] to the direction of flow. Evaluation of these refractive index profiles requires expressions for the radial and axial concentration profiles [$C(r)$ and $C(z)$, respectively] as well as the refractive index dependence on concentration [$n(C)$].

Evaluation of $n(C)$

For ideal solvent systems, refractive index is a simple, linear function of concentration. However, the polar solvents utilized in reversed-phase liquid chromatography are highly interacting and the refractive index commonly exhibits a non-linear concentration dependence[14,15]. For these non-ideal solvent systems, $n(C)$ may play a major role in determining the magnitude as well as the direction of the refractive index gradients present in the flow cell. Since these solutions do not behave ideally and solution theory cannot presently predict the refractive index dependence, experimental measurements of refractive index are necessary. These refractive index measurements can then be described by a polynomial expression for the concentration range of interest.

Evaluation of $C(r)$

The radial concentration profile arises from the flow profile within the flow cell, and may be complex for the Z-pattern cell design[16]. Because these flow patterns are not presently well understood or well characterized, some simplifying assumptions are necessary to model the radial profile. If the flow cell is considered as a simple

cylindrical tube, then the concentration (C) as a function of the radial distance (r) can be expressed as derived by Taylor[17]:

$$C(r) = C_{r=0} + \frac{R^2 u}{4D_M}\left[\frac{r^2}{R^2} - \frac{r^4}{2R^4}\right]\frac{dC_{r=0}}{dz} \tag{1}$$

Thus, the radial concentration profile for a cell of radius (R) depends on the linear velocity in the cell (u) and the diffusion coefficient (D_M), as well as the axial gradient at the center of the cell ($dC_{r=0}/dz$). If the residence time in the cell is short, the concentration profile may be modelled as a parabola by neglecting the $r^4/2R^4$ term.

Evaluation of C(z)

The axial concentration profile arises due to the convolution of the initial concentration profile with the Gaussian dispersion introduced by the chromatographic column or connecting tubing. Dispersion may be determined from the Van Deemter[18] or Knox[19] equations for packed chromatographic columns or the Golay[20] or Taylor–Aris[17,21] equations for open-tubular columns. Finally, evaluation of the concentration profile reaching the detector may be solved mathematically either by Laplace transforms[22] or by convolution of integrals[23].

In the convolution of integrals method, the input concentration profile is convolved directly with the Gaussian function. The input concentration as a function of time [$C(t_a)$] may be described by the initial concentration (C_0) and characteristic time constant (τ). In addition, this input profile is offset by the difference in time (t_R) between the profile introduction and evaluation. The convolution of the input function with a normalized Gaussian operator results in a final concentration function of the following form[23]:

$$C(t) = \frac{1}{(2\pi)^{1/2}\sigma_t}\int_{\substack{\text{all } t_a \\ \text{values}}} C(t_a)\exp\left[-\frac{(t-t_a)^2}{2\sigma_t^2}\right]dt_a \tag{2}$$

where σ_t^2 is the time variance contributed by the chromatographic system. This final concentration profile with respect to time [$C(t)$] is then evaluated by integrating over all possible values of input time (t_a). Subsequent conversion from the time to the distance domain is performed, yielding the final concentration profile with respect to distance [$C(z)$].

A number of input concentration profiles of importance for liquid chromatographic applications are created upon injection as well as by solvent programming. Under ideal injection conditions, the solute enters the chromatographic column as an instantaneous concentration pulse. Alternately, the solute may be swept onto the column in a rectangular plug determined by the length of the injection loop and the linear velocity of the mobile phase. Under less ideal circumstances, the injector may act as a mixing or dilution chamber, and an exponential concentration profile is introduced onto the column. Finally, the separation of complex mixtures often requires programming the mobile phase in a stepwise or linear manner, from the weak to the strong solvent. Each of these profiles will be investigated in turn, with the mathematical derivations and final concentration profiles given in the Appendix.

Evaluation of n(r) and n(z)

Expressions for the concentration profiles in both the radial [$C(r)$] and the axial [$C(z)$] direction as well as the refractive index dependence on concentration have been derived. Thus, determination of refractive index profiles in both radial and axial directions is now possible for the input profiles of interest in liquid chromatography. Unfortunately, the explicit determination of the transmittance expressions as a function of time is not trivial and often they cannot be solved in closed form[24]. In addition, transmittance expressions must be solved individually for each input function and each concentration dependence on refractive index. For these reasons, a modelling approach has been utilized for the prediction of detector response for these gradient conditions. By directly comparing the predicted response with experimental observations, a better understanding of the origin of this refractive index artifact is possible.

EXPERIMENTAL

Reagents

All organic solvents utilized in this study are high-purity, distilled-in-glass grade (Burdick and Jackson, Muskegon, MI, U.S.A.). Water is deionized and doubly distilled (Model MP-3A, Corning Glass Works, Corning, NY, U.S.A.).

Refractive index measurements

Refractive index measurements for binary mixtures of tetrahydrofuran–water and methanol–water are performed at 25°C with an Abbe refractometer (Model Abbe-3L, Bausch and Lomb, Rochester, NY, U.S.A.). Replicate measurements of a single sample, as well as replicate samples, yield a relative standard deviation better than $\pm$ 0.0001. Polynomial expressions from non-linear least squares fitting of refractive index as a function of concentration are given in eqns. 3 and 4, and are shown graphically in Fig. 1. The coefficients of determination for the tetrahydrofuran–water and methanol–water systems are 0.980 and 1.42, respectively.

Chromatographic system

Solvent delivery and gradient introduction are accomplished utilizing a dual-syringe micropump (MPLC Model MG, Applied Biosystems, Santa Clara, CA, U.S.A.). Both internal and external loop injection valves (Model CI4W1 and EC6W, Valco, Houston, TX, U.S.A.) are utilized for sample introduction. External loops are fabricated from stainless steel tubing 0.25 mm I.D. with lengths of 11.8 cm (5.98 μl), 19.7 cm (9.98 μl), 39.5 cm (20.0 μl) and 98.6 cm (50.0 μl). A stainless steel tube (46.0 cm $\times$ 0.25 mm I.D.) is used to connect the injector directly to the absorbance detector (Model Uvidec 100-V, Jasco, Tokyo, Japan). The detector, equipped with a 1-μl Z-pattern flow cell (5 mm $\times$ 0.50 mm I.D.), is operated at a monochromator wavelength of 589 nm with a 500 nm cutoff filter. A chart recorder (Model 585, Linear Instruments, Reno, NV, U.S.A.) is utilized to display the apparent absorbance caused by the refractive index artifact.

Simulations

The flow cell, modelled as a dynamic lens, is simulated utilizing a three-dimensional ray-tracing algorithm (Beam3, Stellar Software, Berkeley, CA, U.S.A.). This software package allows refracting and reflecting optical elements to be

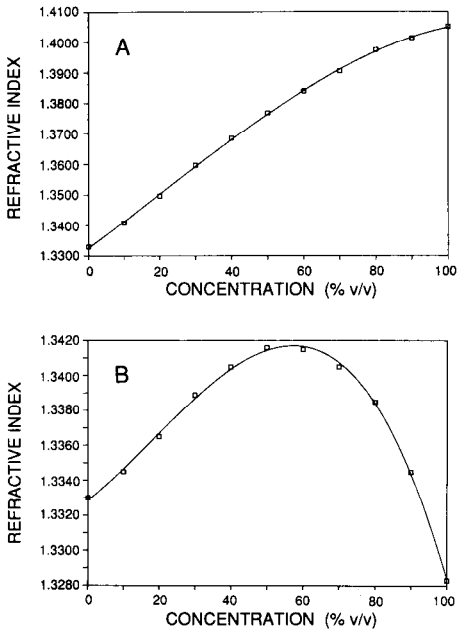

Fig. 1. Refractive index measurements as a function of the concentration of tetrahydrofuran in water (A) and the concentration of methanol in water (B).

arbitrarily positioned and their shape specified. In simulating the Z-pattern cell (Fig. 2), a point source is positioned 0.5 mm in front of the cell entrance and a detection screen is positioned 25.4 mm after the cell exit. Flat refracting elements (n_D = 1.457) representing the quartz cell windows are placed 1.0 mm apart at flow cell entrance and

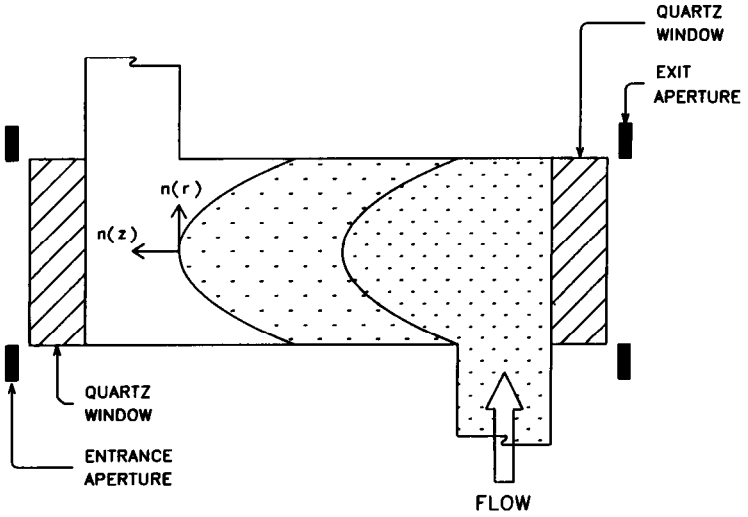

Fig. 2. Schematic diagram of Z-pattern flow cell with refractive index profiles radial [$n(r)$] and axial [$n(z)$] to the direction of flow.

exit, together with apertures of 0.5 mm diameter. The window interfaces inside the cell are positioned 5.0 mm apart, with parabolic refractive index interfaces placed 2.0 and 4.0 mm from the exit window. This parabolic radial profile remains constant while the axial gradient in the cell varies, dependent upon the input profile of interest (eqns. 12, 16, 20 and 24). The axial refractive index profile is incremented through the cell in a stepwise manner, with only a small fraction of the total profile contained in the cell at any given time. The detector response is then predicted by analyzing the image size and intensity at each step. Image size is determined by evaluating the final position of a single peripheral ray at the detector screen. Image intensity is predicted by evaluating the number of rays (I) successfully traversing the cell from 1000 incident rays (I_0). The predicted intensity is then normalized to the mobile phase solvent and the apparent absorbance is subsequently calculated as $[-\log(I/I_0)]$. The relative error in the predicted apparent absorbance is approximately 6% for simulations utilizing at least 500 incident rays. At present, the precision of the simulation model is limited by the reproducibility of the random number generator and is not improved by increasing the number of incident rays.

Implementation of this model requires knowledge of $n(C)$, as well as both $C(r)$ and $C(z)$ expressions. In these studies, reversed-phase solvent systems are chosen which exhibit nearly ideal, linear dependence of refractive index on concentration (tetrahydrofuran–water) as well as distinctly non-ideal behavior (methanol–water). Refractive indices for aqueous, binary mixtures of tetrahydrofuran and methanol are measured and the best fit polynomial expressions are calculated. For binary solutions of tetrahydrofuran and water, the refractive index relationship is given by

$$n(C) = 1.3326 + 0.08561C + 0.02146C^2 - 0.03475C^3 \tag{3}$$

where the concentration (C) is the volume fraction of tetrahydrofuran in the total volume. As can be seen in Fig. 1, aqueous mixtures of tetrahydrofuran exhibit a relatively linear refractive index response with concentration, showing only slight deviation at high concentrations. In contrast, mixtures of methanol and water, as given by

$$n(C) = 1.3329 + 0.01599C + 0.02521C^2 - 0.04568C^3 \tag{4}$$

show a maximum in refractive index with concentration (Fig. 1). These two extremes in refractive index behavior test the versatility of the model for solvents of interest in practical applications.

Secondly, the $C(r)$ expression is necessary to determine the curvature of the "solvent lens". Since the flow pattern within the Z-pattern cell is hydrodynamically complex, calculations of the radial profile are not amenable to an analytical solution. Therefore, assumptions about the shape resulting from a more simplified flow profile are required. The radial profile is modelled as a parabolic profile utilizing the Taylor expression (eqn. 1), neglecting the $r^4/2R^4$ term. The shape and curvature of surfaces of constant concentration and hence refractive index, are given by $[(C - C_{r=0})/(\mathrm{d}C_{r=0}/\mathrm{d}z)]$. Thus, the curvature of the parabolic solvent lens, given by $(R^2u/4D_M)$, remains constant for specified flow conditions. All simulations assume a volumetric flow-rate of 50 μl/min, yielding a mobile phase linear velocity (u) of 0.424 cm/s for the flow cell

radius (R) of 0.25 mm. A diffusion coefficient (D_M) of approximately $1 \cdot 10^{-5}$ cm^2/s is determined from the Wilke–Chang equation[25] for both tetrahydrofuran–water and methanol–water mixtures at 25°C. Because the flow-rate and solvents utilized for these simulations are constant, the parabolic lens shape and curvature remain the same for all simulations.

Finally, the $C(z)$ expression must be evaluated for the experimental conditions of interest if direct comparison of simulated results with experimental observations is desired. Therefore, simulation input parameters are obtained directly from the experimental conditions whenever possible. The actual concentration expressions are derived in the Appendix using the convolution of integrals method and are given in eqns. 12, 16, 20 and 24. This technique requires information about the Gaussian operator as well as the input function of interest.

In these studies, the initial concentration profile is generated experimentally by either an injection valve or a gradient dual-syringe pump. The Gaussian operator is experimentally formed utilizing a non-retentive open tube. Direct connection between the detector flow cell and the injection valve or gradient pump is accomplished with stainless steel tubing. Since the solvents are unretained, the time to traverse the tube (t_R) is the ratio of the distance travelled (L = 46.0 cm) to the linear velocity (u = 1.64 cm/s) and is equal to 27.1 s. The length variance (σ_L^2) contributed by this tube is calculated from the Taylor–Aris expression[17,21].

$$\sigma_L^2 = R^2u/24D_M \tag{5}$$

For the experimental conditions described, the connecting tube contributes a length variance of 50.8 cm^2 and a corresponding time variance of 18.9 s^2. If no additional broadening occurs between the connecting tube (R = 0.127 mm) and the flow cell (R = 0.250 mm), the time variance is assumed constant and the length variance in the cell is 3.40 cm^2 at a corresponding linear velocity of 0.424 cm/s in the cell.

A number of axial concentration profiles commonly encountered in liquid chromatography have been investigated to test the validity of the simulation model. Mathematical expressions for these input functions as well as the axial concentration profiles determined by convolution of integrals are given in the Appendix. For simulations of the exponential input function (eqn. 12), the ratio of the exponential time constant (τ) and the Gaussian standard deviation (σ_t) are varied from an ideal Gaussian function (τ/σ_t = 0.00) to the exponentially modified Gaussian (τ/σ_t = 0.25–2.00). The axial concentration expression resulting from a more ideal, rectangular plug injection (eqn. 16) is also of interest. For these simulations, injection volumes of 1, 6, 10, 20 and 50 μl are investigated. The time of the rectangular injection (τ) is calculated from the ratio of the injection loop length (L_{inj}) and linear velocity (u). The injection loop diameter was chosen to be equal to the connecting tube diameter, to minimize any dispersion due to transfer between the tubes and thus the linear velocity remains constant. The length of injection loops results in τ/σ_t ratios of 0.297, 1.78, 2.97, 5.94 and 14.9, corresponding to the various injection volumes. This produces a wide range of axial concentration profiles at the detector from a nearly Gaussian profile for the 1-μl injection to an almost rectangular profile for the 50-μl injection. The concentration profile formed for step gradient input is given in eqn. 20. For these simulations, a solvent program from 0 to 100% (v/v) is evaluated which employs 10 steps (m) of 10% (v/v) increment at a step time interval (τ) of 5 min. A comparable

linear gradient (eqn. 24) from 0 to 100% (v/v) in 45 min (τ) is also calculated. Finally, these axial concentration gradients are combined with the expressions for $n(C)$ to determine the axial refractive index profile utilized as input to the simulation model.

RESULTS AND DISCUSSION

In an effort to understand the origin of the refractive index artifact in absorbance detection, the response of a commercially available detector is measured under both injection and solvent programming conditions. These measurements are then compared with predictions of the apparent absorbance based on the "dynamic lens" model. Because the refractive index artifact is simulated for the flow conditions used experimentally, direct comparison of theoretical prediction with experimental observation is possible. In addition, one solvent system with a nearly ideal, linear refractive index dependence on concentration (tetrahydrofuran–water) is contrasted with a distinctly non-ideal system (methanol–water). This direct comparison of complex input profiles and solvent systems tests the versatility and applicability of this "dynamic lens" model for the elucidation of this important artifact of absorbance detection.

δ input function

While the δ input function was addressed in a previous publication[11], the conclusions are summarized here for completeness. A δ function input, when convolved with a Gaussian operator, results in a purely Gaussian concentration profile. For the linear change in refractive index exhibited for small changes in concentration, the axial refractive index profile is also Gaussian in shape. Both the predicted and experimentally observed response show the characteristic derivative-shaped signal for image diameter as well as image intensity. At the beginning of the Gaussian profile, both the axial and radial refractive index gradients are positive, thereby focussing the incident radiation. In the second half of the profile, the axial gradient is negative while the radial gradient remains positive, effectively defocussing the final image. Since the exit to the flow cell acts as the aperture stop under simulation as well as experimental conditions, the amount of light blocked by the flow cell exit changes continuously with the axial gradient within the cell. Thus, the "solvent lens" in the cell and the limiting aperture after the cell combine to yield the apparent derivative shape of the detector response, whether expressed as image intensity or apparent absorbance.

Exponential input function

The time-dependent concentration profiles calculated for the exponential input function convolved with the Gaussian function operator (eqn. 8), are shown graphically in Fig. 3. As expected, an increasing exponential modification (increased τ/σ_t) reduces the maximum concentration present at the detector. This reduction in the concentration maximum results in a concomitant decrease in the magnitude of the concentration gradient (dC/dz) in the flow cell.

Predicted detector response for these concentration profiles, measured at the first and second deflection of the derivative-shaped curve, is summarized in Table I for the injection of 1 μl tetrahydrofuran into water. The predicted deflection maximum

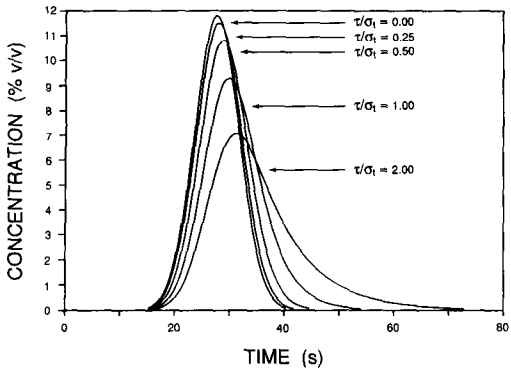

Fig. 3. Calculated concentration dependence, based on eqn. 11, for a Gaussian profile with variance σ_t^2 modified by a varying exponential time constant (τ).

occurs when the refractive index gradient in the cell (dn/dz) reaches a maximum value. For this reason, the refraction index gradient is tabulated together with the corresponding image diameter and apparent absorbance at each deflection maximum. For the ideal Gaussian function ($\tau/\sigma_t = 0$), the predicted image diameter exhibits an approximately symmetric response (-0.16 then $+0.17$) relative to that for pure water (1.00). In contrast, the magnitude of the apparent absorbance is greater for the first deflection (-0.15) than the second ($+0.10$). For the first deflection, the axial and radial refractive index gradients are positive and the incident light is refracted toward the cell axis, thereby increasing light transmitted and decreasing the apparent absorbance. Because light is refracted toward the cell axis under these conditions, light rays can traverse the cell at a radial position further from the cell axis than for a negative axial gradient. At these radial positions, the parabolic profile forms a much steeper refractive index gradient and more light can be transmitted. However, when the axial gradient is negative, light is refracted away from the axis and must traverse the cell at a radial position nearer the cell axis to pass through the exit aperture. In this case, the portion of the radial profile encountered by light rays is less steep and the light

TABLE I

PREDICTED RESPONSE FOR EXPONENTIALLY MODIFIED GAUSSIAN PROFILE UTILIZING THE TETRAHYDROFURAN–WATER SYSTEM

τ/σ_t	dn/dz (mm^{-1}) × 10^3		*Relative image diameter*		*Apparent absorbance*	
	1st[a]	*2nd*[b]	*1st*[a]	*2nd*[b]	*1st*[a]	*2nd*[b]
0.00	0.29	−0.29	0.841	1.168	−0.15	0.10
0.25	0.28	−0.27	0.846	1.158	−0.14	0.09
0.50	0.25	−0.23	0.860	1.135	−0.13	0.08
1.00	0.21	−0.16	0.885	1.094	−0.09	0.05
2.00	0.15	−0.08	0.919	1.049	−0.05	0.01

[a] Maximum value at first deflection relative to pure water.
[b] Maximum value at second deflection relative to pure water.

is refracted to a lesser extent. This asymmetry in refractive index conditions encountered within the cell results in an asymmetry in the magnitude of the detector response, even for a symmetric axial profile. Thus, in contradiction to previous assumptions[10], the existence of asymmetry in the refractive index artifact may not necessarily be indicative of an asymmetric axial profile.

As the τ/σ_t ratio increases, the magnitude of the concentration gradient (dC/dz) decreases for both the positive and negative axial gradient. However, the magnitude of the negative gradient decreases more rapidly than the positive gradient, as can be discerned from the slope of the profiles in Fig. 3. This difference in the concentration gradient at the front and back of the profile is a direct result of the asymmetry of the exponential function. This asymmetry in the concentration profiles is directly reflected in the refractive index profiles for the tetrahydrofuran–water system. As can be seen in Table I, the relative image diameter predicted at the first and second deflection of the derivative-shaped response likewise increases in asymmetry with increasing τ/σ_t ratio. This results in a concomitant increase in the asymmetry of the predicted apparent absorbance with increasing τ/σ_t ratio. If the exponential modification is sufficiently great, as shown for a τ/σ_t ratio of 2.00, the second deflection is no longer detected and the resulting apparent absorbance response appears as a unidirectional peak. Simulations of the exponential input function have been discussed only for the tetrahydrofuran–water system to isolate the change in positive and negative gradient occurring for varying τ/σ_t ratios. Experimental verification of the detector response was not attempted due to the difficulty in matching τ/σ_t values.

In summary, an inherent asymmetry in the apparent absorbance is predicted for a symmetrical Gaussian axial gradient. This asymmetry in detector response increases as τ/σ_t ratio increases, due to the growing asymmetry in the positive and negative gradient portions of the axial profile. If the exponential contribution to the axial profile becomes too great, the second deflection may not be detected. Thus, the shape as well as the magnitude of the detector response are directly affected by the exponential input function.

Rectangular input function

Detector response has also been predicted for the rectangular input function which might occur upon plug injection. Rectangular injections of 1, 6, 10, 20 and 50 μl

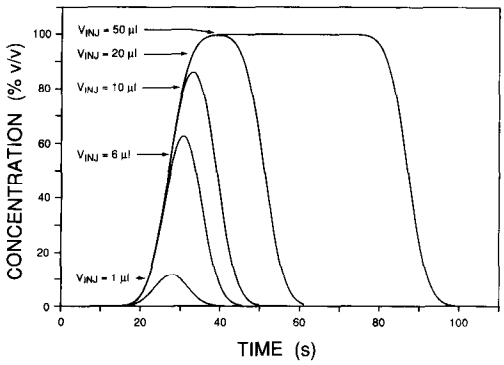

Fig. 4. Calculated concentration dependence, based on eqn. 15, for a Gaussian profile with variance σ_t^2 modified by a varying rectangular injection volume.

have been simulated utilizing the concentration profiles calculated from eqn. 16. The time-dependent concentration profiles (eqn. 15) resulting from the convolution of a rectangular input function with a Gaussian operator are shown in Fig. 4. Both tetrahydrofuran–water and methanol–water systems are employed to evaluate the effect of ideal as well as non-ideal solvent mixtures on the detector response.

Predicted response for injections of tetrahydrofuran into water are shown in Fig. 5. For a 1-μl injection of tetrahydrofuran into water, Fig. 5-1A illustrates the axial refractive index profile utilized as input to the simulation model. The axial profile shows a nearly Gaussian shape, where the refractive index gradient (Fig. 5-1B) is first positive and then becomes negative. The positive portion of the refractive index gradient coupled with the positive parabolic radial gradient causes light to be refracted toward the center of the flow cell. This focussing of the incident light results in the initial decrease in the image diameter (Fig. 5-1C) relative to that for pure water. A concomitant decrease in the apparent absorbance (Fig. 5-1D) is seen because more light is allowed through the flow cell exit which is acting as the system aperture stop. The opposite effect results when the axial gradient becomes negative; that is, the light is now refracted away from the flow cell center and thus the image diameter increases. Because more light is now blocked by the exit aperture, the apparent absorbance increases. These continually changing refraction conditions give rise to the characteristic derivative-shaped response.

As the volume is increased to 6 μl of tetrahydrofuran injected into water, the axial refractive index profile (Fig. 5-6A) increases in magnitude but remains approximately Gaussian in shape. The shape and direction of the resulting refractive index gradient (Fig. 5-6B) are the same as shown for a 1-μl injection, but the magnitude of the gradient has increased. The predicted image diameter (Fig. 5-6C) resulting from the gradient has also increased in magnitude but remained the same in all other respects. In contrast, the overall magnitude of the predicted apparent absorbance (Fig. 5-6D) has increased, but the predicted response reaches a plateau as the apparent absorbance decreases. This appears to be the direct result of the increased focussing power of the "solvent lens"; that is, dn/dz increases to such an extent that the exit of the flow cell no longer limits the light transmitted through the cell. At these high gradients, the light is focussed enough so the aperture stop gradually moves toward the entrance of the cell, until the cell entrance acts as both the aperture and field stop. When the limiting apertures are preceding the solvent lens, the apparent absorbance is no longer a function of the axial refractive index gradient and therefore, remains constant within this time region.

As the injection volume is increased to 10 μl of tetrahydrofuran into water, the refractive index profile (Fig. 5-10A) increases only slightly in magnitude and becomes less Gaussian in shape. Although the refractive index gradient (Fig. 5-10B) is only slightly greater than for the 6-μl injection, the plateau effect in the predicted apparent absorbance (Fig. 5-10D) is even more pronounced because more time is spent under these high gradient conditions. For a 20-μl injection of tetrahydrofuran into water, the concentration, and thus the refractive index (Fig. 5-20A), has reached a maximum value equal to that for pure tetrahydrofuran. This results in a time interval between steep gradient regions when dn/dz (Fig. 5-20B) equals zero. The steep gradient regions are approximately equal in magnitude to that for a 10-μl injection (Fig. 5-10B), but are now distinctly separated in time. This separation is reflected in both the predicted

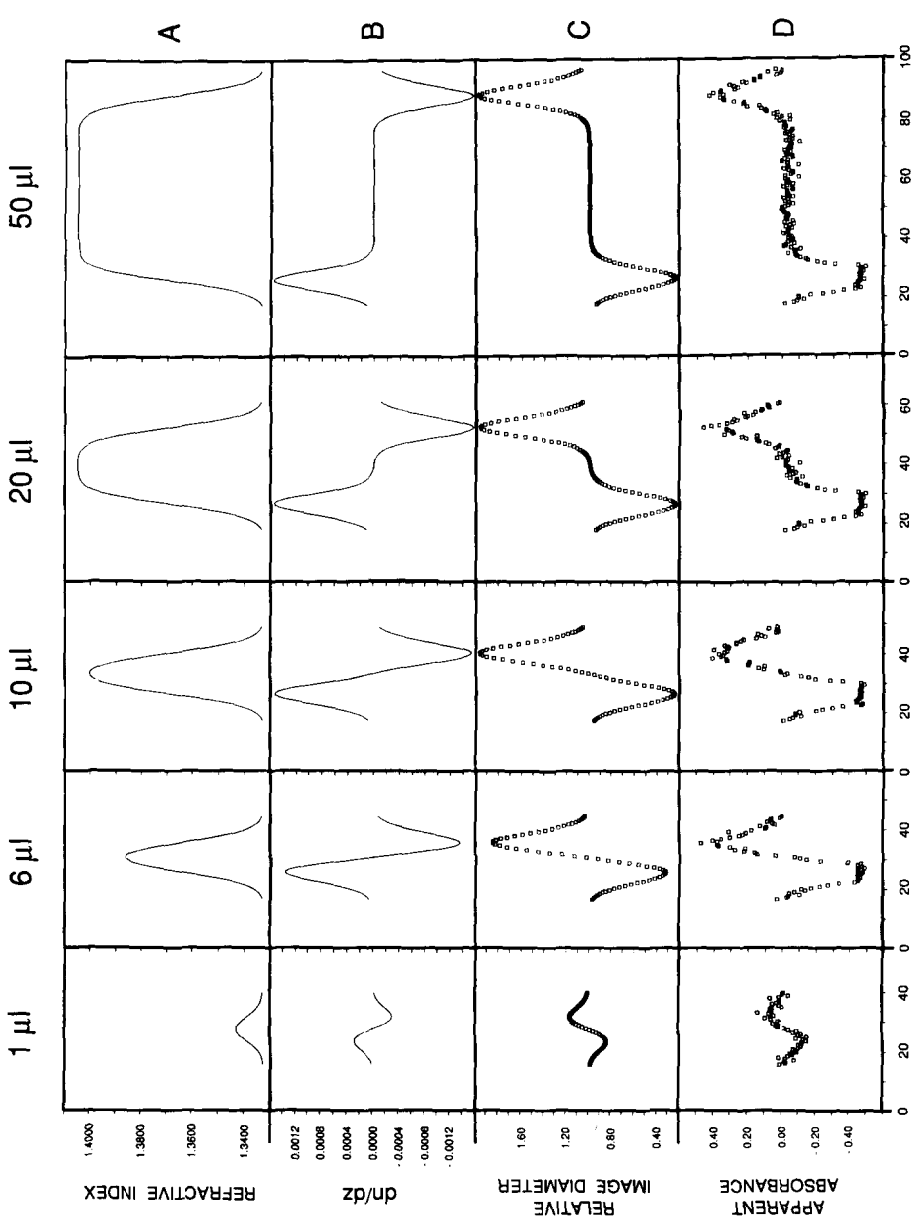

Fig. 5. Calculated absolute refractive index (A) and refractive index gradient (B) in the cell (mm^{-1}), and resultant relative image diameter (C) and apparent absorbance (D) predicted for varying volumes of tetrahydrofuran injected into water.

image diameter (Fig. 5-20C) and the apparent absorbance (Fig. 5-20D). In an actual chromatogram, it would be difficult to determine whether the detector response arose from the refractive index artifact or was the true absorbance response from two independent solutes. This distinction would become nearly impossible for the 50-μl injection of tetrahydrofuran into water, where the predicted response is well separated in time (Fig. 5-50D). Thus, although a single component is injected, the predicted response is difficult to distinguish from two independent chromatographic peaks for large injections of these ideal solvents.

Experimental observations for the tetrahydrofuran–water system are shown in Fig. 6. The experimental concentration profile (Fig. 6A), measured with an absorbing solute, is nearly Gaussian in shape for 1- and 6-μl injections, and reaches the maximum possible concentration for 20- and 50-μl injections. The corresponding refractive index artifacts are shown for a 20% (v/v) mixture of tetrahydrofuran–water injected into pure water (Fig. 6B), due to complications in hydrodynamic mixing for injections of a pure organic solvent into pure water. Excellent agreement with predicted response (Fig. 5) is seen for the shape of the observed apparent absorbance for the tetrahydrofuran–water system. Although an increase in magnitude of the apparent absorbance is predicted with increasing injection volume, a slight decrease is observed experimentally in some cases for reasons which are not clear. In general, however, the trend in the shape, direction, and relative magnitude corresponds directly with that predicted by the "dynamic lens" model.

Further investigation of this absorbance anomaly employed the less ideal methanol–water solvent system. As described previously, mixtures of methanol and water interact in such a way to give a maximum in the refractive index dependence on concentration (Fig. 1B). However, predicted response behavior for injections of 1 μl of methanol into water, shown in Fig. 7, are similar to those for the tetrahydrofuran–water system (Fig. 5). Although the magnitude of the image diameter response (Fig.

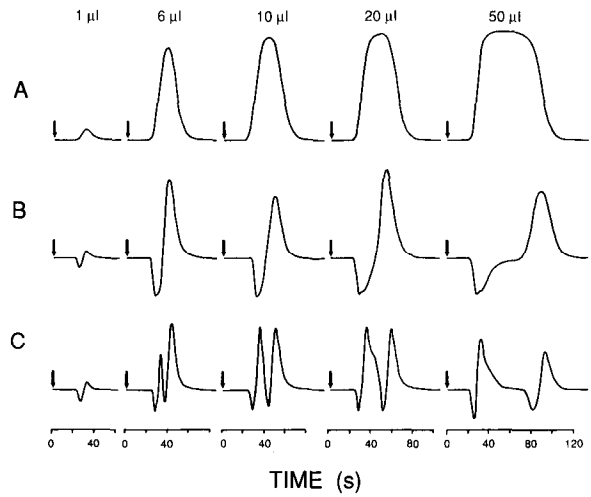

Fig. 6. Observed detector response (λ = 250 nm) for injection of varying volumes of 1% (v/v) acetone–methanol into methanol (A); 1.500 a.u.f.s. Apparent absorbance observed (λ = 589 nm) for injection of 20% (v/v) tetrahydrofuran–water into water (B) and 90% (v/v) methanol–water into water (C); 0.200 a.u.f.s.

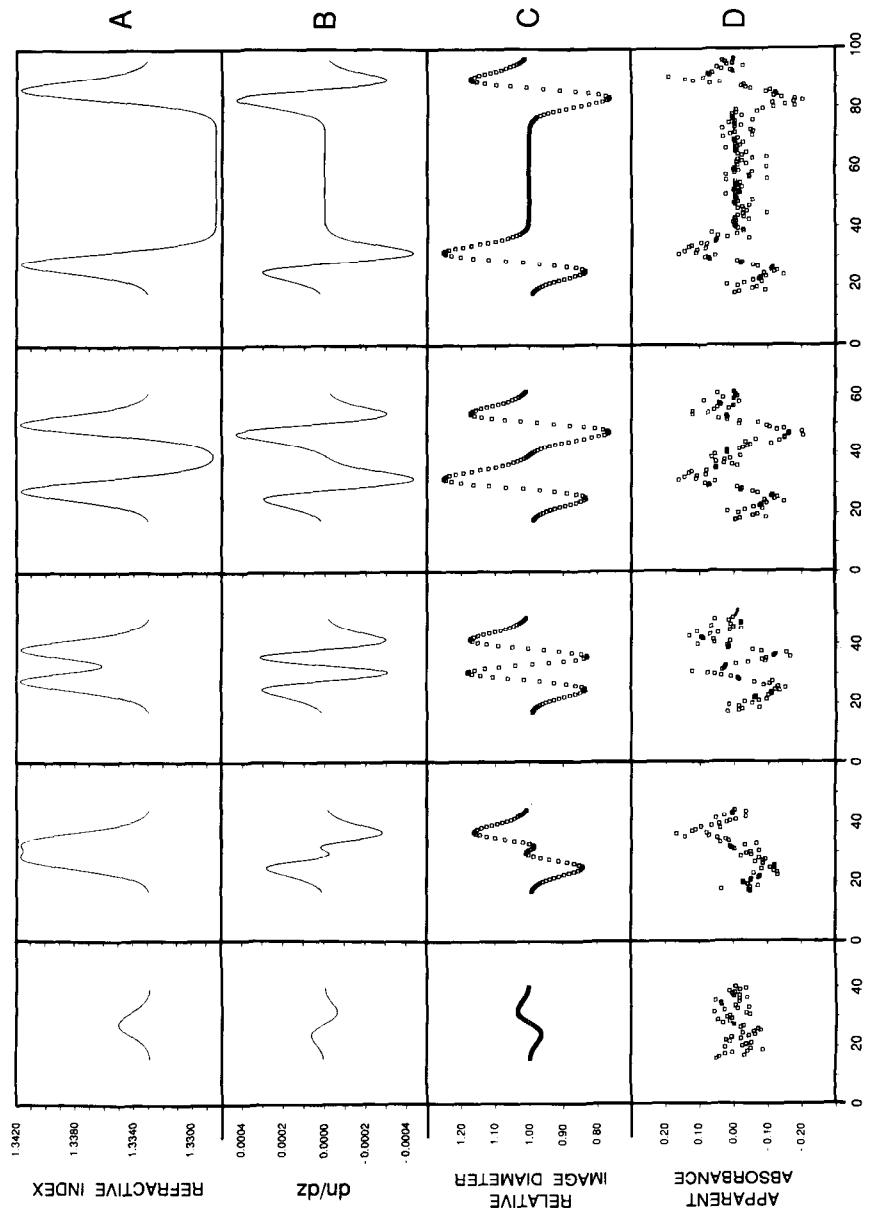

Fig. 7. Calculated absolute refractive index (A) and refractive index gradient (B) in the cell (mm^{-1}), and resultant relative image diameter (C) and apparent absorbance (D) predicted for varying volumes of methanol injected into water.

7-1C) is smaller than for tetrahydrofuran injected into water, the shape and direction of the response are identical. The apparent absorbance (Fig. 7-1D) predicted by the model is difficult to discern due to variability in the random number generator utilized in the simulation.

The non-linearity of refractive index with concentration becomes more important as the injection volume increases. This can be seen for the 6-μl injection of methanol into water, where the magnitude of the refractive index profile (Fig. 7-6A) has increased but the shape is distinctly non-Gaussian. This unusual refractive index profile results because the maximum in the concentration profile is greater than 50% (v/v) (Fig. 4), and thus, is slightly greater than the maximum in the refractive index *versus* concentration relationship (Fig. 1B). This results in a small decrease in the refractive index profile at the concentration maximum. The refractive index gradient (Fig. 7-6B), in this case, is beginning to exhibit multiple changes in sign, giving rise to an unusual shape in the predicted image diameter (Fig. 7-6C). The predicted apparent absorbance (Fig. 7-6D), however, appears to exhibit only two deflections, presumably due to the variability in the random number generator used for the simulation.

The non-linearity of refractive index with concentration continues to influence the refractive index profile for injections of 10 μl of methanol into water. Since the maximum in the concentration profile is greater than 80% (v/v), substantially past the maximum in the refractive index *versus* concentration relationship, a bimodal refractive index profile results (Fig. 7-10A). The axial refractive index gradient (Fig. 7-10B), although comparable in magnitude to the 6-μl injection, clearly shows multiple changes in sign. Predicted image diameter (Fig. 7-10C) and apparent absorbance (Fig. 7-10D) for this injection, likewise change in direction several times as the refractive index profile traverses the cell.

The concentration profile for injection of 20 μl of methanol into water reaches the maximum for pure methanol, resulting in a complex refractive index profile (Fig. 7-20A). The shape of the axial refractive index gradient (Fig. 7-20B) now appears as the derivative of two separate Gaussian refractive index profiles. Thus, the image diameter (Fig. 7-20C) and apparent absorbance response (Fig. 7-20D) predicted by the simulation model show two partially resolved derivative-shaped peaks. Although this response is predicted for a single injection, it is difficult to distinguish from the response arising from the injection of two, more ideal solvents that have been separated by a column.

This difficulty becomes most pronounced for a 50-μl injection of methanol into water. In this case, since the refractive index gradients (Fig. 7-50B) are well separated in time, both the image diameter (Fig. 7-50C) and apparent absorbance (Fig. 7-50D) also exhibit two, apparently separate responses. Thus, the non-linear nature of $n(C)$ can play a major role in determining the shape, direction and magnitude of the apparent absorbance response.

Experimental observations for the injection of 90% (v/v) methanol–water into pure water are shown in Fig. 6C. Excellent agreement is seen in the shape, direction, and relative magnitude of the observed apparent absorbance with that predicted (Fig. 7) for this non-ideal solvent system. The observed response exhibits some asymmetry, not predicted utilizing the ray-tracing model. This observed asymmetry may be caused by small misalignment in the commercial detection system. In addition, deviations from a symmetric, parabolic flow profile may also contribute to the observed

asymmetry. The correlation between the predicted and observed apparent absorbance, however, appears very good for this non-ideal solvent system.

In summary, the refractive index dependence on concentration has a substantial effect on the form of the refractive index profile for large rectangular injections. For a nearly ideal solvent system, large injections can result in an apparent absorbance response which appears as two, separate solute peaks, one negative and one positive. In other cases, it is difficult to distinguish the refractive index artifact caused by the injection of a single, non-ideal component from that caused by a mixture of two ideal components separated by a chromatographic column. This result has important implications for the evaluation of system peaks in liquid chromatography utilizing absorbance detection[26,27]. In fact, the analysis of system peaks may be more complex than has been previously thought.

Stepwise input function

Detector response has also been predicted for the more complex gradients utilized for solvent programming in liquid chromatography. The concentration profile resulting from the convolution of a discontinuous step function with the Gaussian operator is given by eqns. 19 and 20. Refractive index profiles have been calculated and

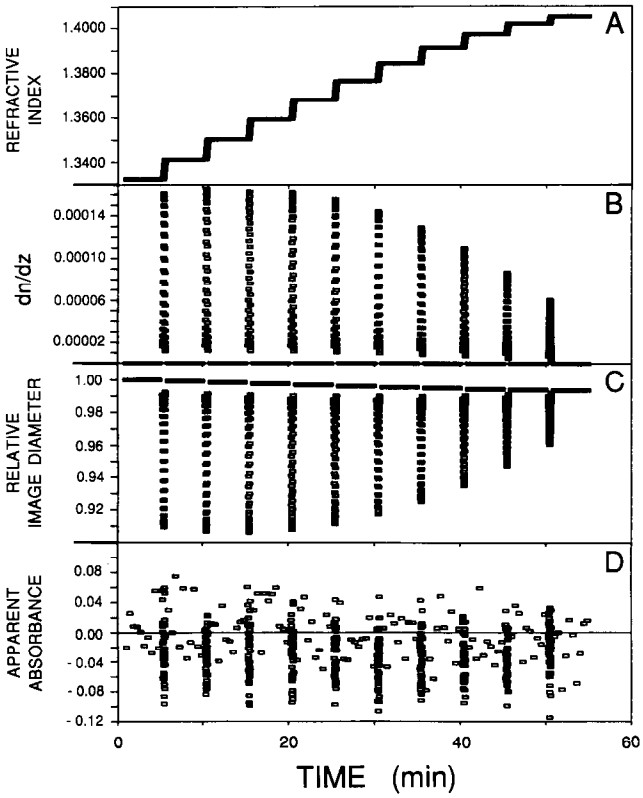

Fig. 8. Calculated absolute refractive index (A) and refractive index gradient (B) in the cell (mm^{-1}), and resultant relative image diameter (C) and apparent absorbance (D) predicted for a stepwise increase of tetrahydrofuran into water from 0 to 100% (v/v) in 10% (v/v) increments.

simulations accomplished for the tetrahydrofuran–water system as well as the methanol–water system.

Predicted detector response for an input function of ten steps of 10% (v/v) tetrahydrofuran in water, from 0 to 100% (v/v), is shown in Fig. 8. Although the concentration increment of the steps is equal, the refractive index profile (Fig. 8A) shows a decrease in step height with increasing concentration of tetrahydrofuran. This decrease in the magnitude of the refractive index steps reflects the slight non-linearity in the refractive index *versus* concentration relationship for high concentrations of tetrahydrofuran in water. This non-linearity results in a marked decrease in the axial refractive index gradient (Fig. 8B) for steps above 50% (v/v). Predicted values for the relative image diameter (Fig. 8C) at each step show the decrease expected for a positive axial refractive index gradient. A direct correspondence can be seen between the magnitude in the axial gradient and the predicted image diameter. In addition, a small decrease in the image diameter at each plateau between steps is predicted due to the change in absolute refractive index. The apparent absorbance (Fig. 8D) predicted for these steps is difficult to see due to scatter in the data caused by the reproducibility of the random number generator. However, changes in apparent absorbance at each step appear to be negative, as is expected from the predicted image diameter (Fig. 8C).

Experimental observations for the tetrahydrofuran–water step gradient, illustrated in Fig. 9B, show excellent agreement with response predicted by the ray-tracing model. As predicted, a negative peak can be seen in the observed apparent absorbance

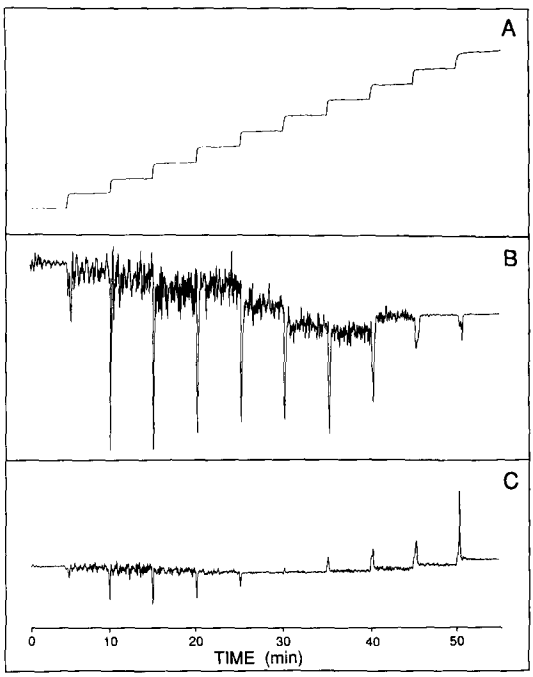

Fig. 9. Observed detector response (λ = 250 nm) for stepwise increase in 1% (v/v) acetone–methanol into methanol from 0 to 100% (v/v) in 10% (v/v) increments (A); 0.160 a.u.f.s. Apparent absorbance observed (λ = 589 nm) for the same stepwise solvent program for 20% (v/v) tetrahydrofuran–water into water (B) and 90% (v/v) methanol–water into water (C); 0.040 a.u.f.s.

at each 10% (v/v) increase in the tetrahydrofuran concentration. In addition, the magnitude of the peaks decreases as the concentration of tetrahydrofuran increases, as predicted by the model (Fig. 8). The apparent noise between steps, which arises from poor mixing, becomes less pronounced at high concentrations of tetrahydrofuran due to the improvement in solvent mixing and the reduction in the refractive index dependence on concentration.

Further simulations of the step function input are shown in Fig. 10 for the non-ideal methanol–water system. A maximum in the refractive index profile (Fig. 10A) is seen for equal steps of 10% (v/v) methanol into water, as expected from the refractive index dependence on concentration (Fig. 1B). This alters not only the magnitude of the axial gradient (Fig. 10B) at each step, but the direction as well. Each step from 0% (v/v) to approximately 50% (v/v) methanol in water shows a positive axial gradient, while steps in the concentration range greater than 50% (v/v) are negative. The change in the direction and magnitude of the axial refractive index gradient are mirrored in the predicted image diameter (Fig. 10C). Predicted apparent absorbance (Fig. 10D) is, again, difficult to discern due to simulation constraints, but it is expected to be similar in direction and shape to the predicted image diameter. Thus, the same stepwise concentration profile exhibits a completely different detector

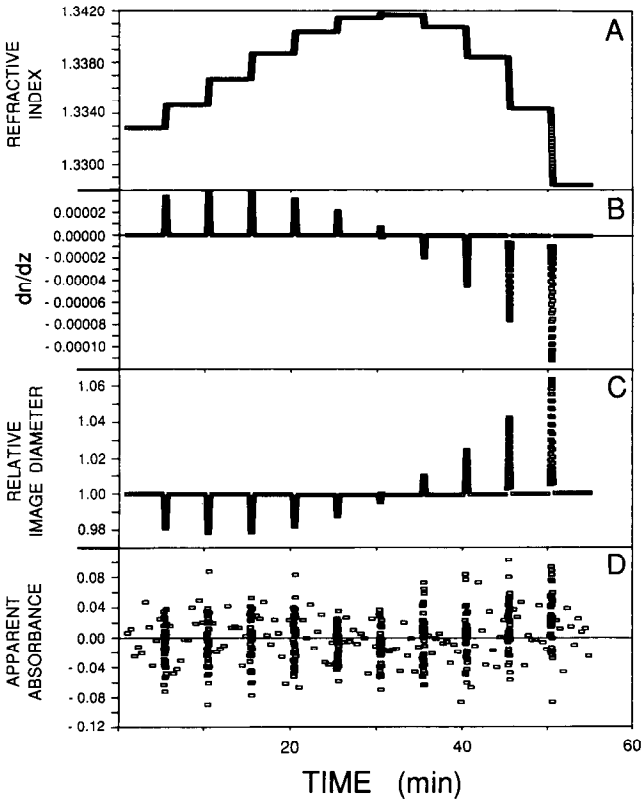

Fig. 10. Calculated absolute refractive index (A) and refractive index gradient (B) in the cell (mm^{-1}), and resultant relative image diameter (C) and apparent absorbance (D) predicted for a stepwise increase of methanol into water from 0 to 100% (v/v) in 10% (v/v) increments.

response for the methanol–water and the tetrahydrofuran–water systems, and the magnitude and direction depend directly on the refractive index *versus* concentration [$n(C)$] relationship.

Experimental observation of the refractive index artifact for the methanol–water system is illustrated in Fig. 9C. The shape and direction of the observed apparent absorbance corresponds directly with that predicted by the "dynamic lens" model. In addition, the relative magnitude of the observed and predicted response are in excellent agreement.

In summary, a complex refractive index artifact often results from a stepwise solvent program. Under these conditions, a steep rise in concentration over a short time results in high axial gradients in concentration and thus refractive index. The refractive index dependence on concentration appears to determine both the magnitude and the direction of the apparent absorbance response. Good agreement is seen between theoretical predictions utilizing this ray-tracing model and experimental observations with a commercially available absorbance detector. As illustrated in Fig. 9, the step gradient input can give rise to apparent absorbance peaks which are often not discernable from analyte absorbance. Moreover, these artifacts frequently occur during a chromatographic analysis where analyte peaks might be expected, as upon a rapid increase in solvent strength.

Linear input function

The input function most often utilized in gradient elution has also been investigated. The concentration profile of the linear input function convolved with the Gaussian operator is given by eqn. 24. For direct comparison with the stepwise function, the linear profile has been simulated for 0 to 100% (v/v) in 45 min (τ).

Simulation predictions are given in Figs. 11 and 12 for the tetrahydrofuran–water system and the methanol–water system, respectively. All axes are the same as for Figs. 8 and 10 to facilitate the direct comparison with step gradient predictions. For both the tetrahydrofuran–water and the methanol–water systems, the overall change in refractive index is identical for the step and linear gradient studies. However, the step profile incorporates several discontinuous changes while the linear profile is continuously changing. This gradual change in concentration for the linear profile results in an axial refractive index gradient (Figs. 11B and 12B) in the flow cell which is approximately two orders of magnitude less than that for the step profile. These small gradients are directly reflected in the magnitude of the predicted detector response for both relative image diameter and apparent absorbance. Thus, only a small baseline offset is predicted for the linear concentration gradient. This result is experimentally observed and shown in Fig. 13 for both tetrahydrofuran–water and methanol–water systems.

In summary, the linear solvent programs commonly utilized in liquid chromatography create only a small axial refractive index gradient in the flow cell. This results in a substantial reduction in the magnitude of the refractive index artifact in comparison to that for the stepwise solvent program. In fact, the linear profiles utilized for gradient elution appear to create a refractive index artifact which is related more to the absolute refractive index than to the refractive index gradient in the flow cell.

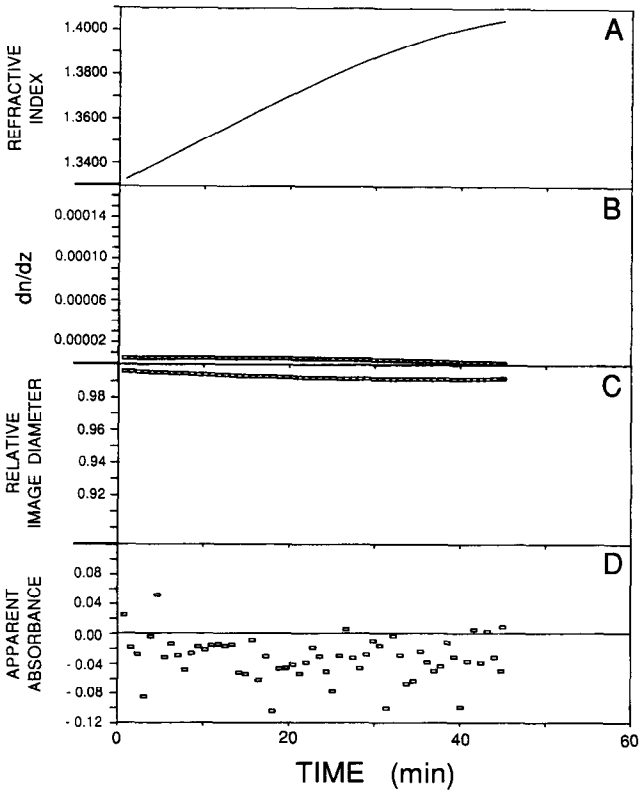

Fig. 11. Calculated absolute refractive index (A) and refractive index gradient (B) in the cell (mm^{-1}), and resultant relative image diameter (C) and apparent absorbance (D) predicted for a linear increase of tetrahydrofuran into water from 0 to 100% (v/v).

CONCLUSIONS

The "dynamic lens" model provides an accurate description of the direction, shape and magnitude of the refractive index artifact under a wide variety of solvent conditions. Excellent agreement between predicted and experimental detector response is observed when refractive index gradients are incorporated with components both radial and axial to the direction of flow. Although the studies described herein utilize equipment and experimental conditions typical of microbore columns, identical detector response is expected for conventional chromatographic systems under comparable hydrodynamic and optical conditions.

For the solvent systems of interest in reversed-phase liquid chromatography, the direction and magnitude of the refractive index gradients are directly dependent on the refractive index *versus* concentration relationship. In the case where both the axial and radial refractive index gradients are positive, the incident light is focussed by the "dynamic lens" and the final image size decreases. If the limiting aperture resides at the flow cell exit, this decrease in the image size allows more energy to be transmitted through the cell, resulting in a decrease in the apparent absorbance. However, if the

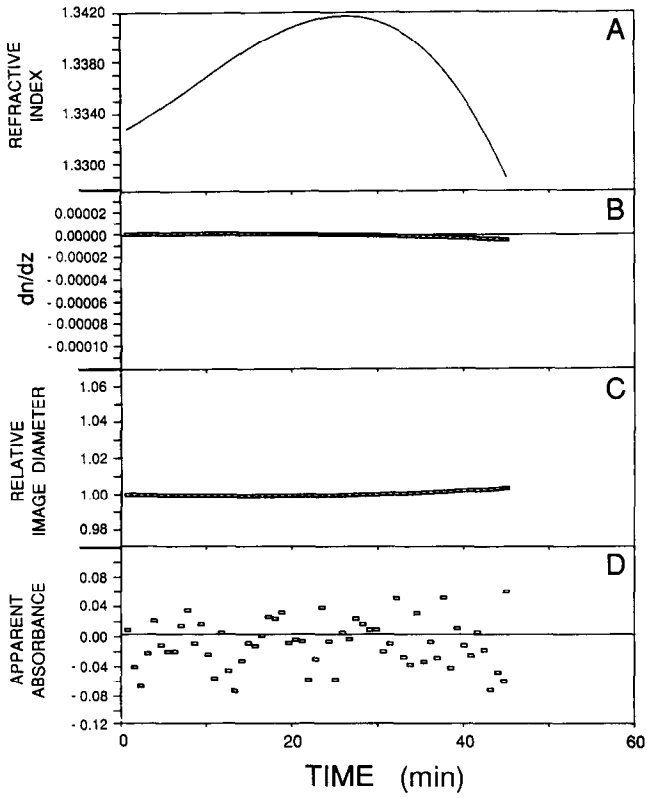

Fig. 12. Calculated absolute refractive index (A) and refractive index gradient (B) in the cell (mm^{-1}), and resultant relative image diameter (C) and apparent absorbance (D) predicted for a linear increase of methanol into water from 0 to 100% (v/v).

axial gradient is negative while the radial gradient remains positive, the incident light is defocussed and the final image size increases. This causes less energy to strike the photodiode and thus an increase in the apparent absorbance is observed. The position of the limiting aperture in the optical system ultimately determines whether the change in image size caused by the refractive index gradients will result in a change in the apparent absorbance. In addition, both axial and radial refractive index gradients must be present within the cell volume for this focussing effect to be observed.

These optical conditions must all be considered when evaluating the observed refractive index artifact. Because no single factor determines the apparent absorbance response at the photodiode, characterization of this artifact requires detailed knowledge of the optical configuration as well as the refractive index conditions present within the flow cell. With this understanding, it becomes possible to eliminate this refractive index artifact in absorbance detection or, alternatively, to optimize refractive index detectors which are based on this response. This understanding is also necessary for the accurate evaluation of system peaks, which are often measured directly from the apparent absorbance response observed upon the injection of a mixture of solvents. Thus, optical simulation of refractive index effects can aid in the

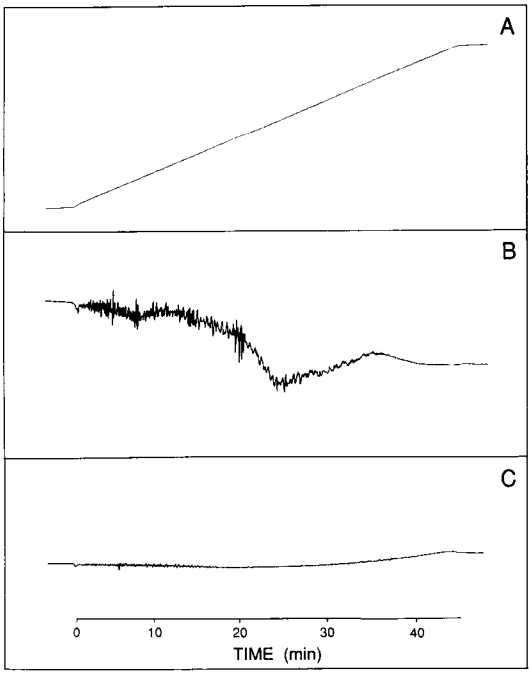

Fig. 13. Observed detector response (λ = 250 nm) for a linear increase in 1% (v/v) acetone–methanol into methanol from 0 to 100% (v/v) (A); 0.160 a.u.f.s. Apparent absorbance observed (λ = 589 nm) for the same linear solvent program for 20% (v/v) tetrahydrofuran–water into water (B) and 90% (v/v) methanol–water into water (C); 0.040 a.u.f.s.

design of improved detectors for liquid chromatography, as well as the more accurate evaluation of fundamental parameters of chromatographic separations. Although the "dynamic lens" model is illustrated here for the evaluation of refractive index artifacts in the Z-pattern flow cell, these ray-tracing simulations may be applied to the evaluation of any optical flow cell design where refractive index is an important factor in the detector response.

APPENDIX

Evaluation of the refractive index profiles present in the flow cell requires the calculation of the final axial concentration as a function of time and distance, $C(t)$ and $C(z)$, respectively. The axial concentration profiles necessary for the simulations are derived below for injection and gradient elution conditions common in liquid chromatographic separations.

Exponential input function

Under non-ideal injection conditions, the input concentration function which results from the injection of an initial concentration (C_0) has the form,

$$C(t_a) = C_0 \exp\left[-\frac{(t_a - t_R)}{\tau}\right] \qquad \text{for } t_R \leqslant t_a \leqslant \infty \tag{6}$$

where the time constant (τ) is characteristic of the size and flow conditions present in the chamber and t_R is the time delay between the injector and detector. The concentration profile at the column exit [$C(t)$] may be evaluated for the exponential input by substituting eqn. 6 into eqn. 2.

$$C(t) = \frac{1}{(2\pi)^{1/2}\sigma_t} \int_{t_R}^{\infty} C_0 \exp\left[-\frac{(t_a - t_R)}{\tau}\right] \exp\left[-\frac{(t - t_a)^2}{2\sigma_t^2}\right] dt_a \tag{7}$$

Expansion and rearrangement of eqn. 7 yields

$$C(t) = \frac{C_0}{(2\pi)^{1/2}\sigma_t} \exp\left[-\frac{(t - t_R)}{\tau}\right] \exp\left(\frac{\sigma_t^2}{2\tau^2}\right) \int_{t_R}^{\infty} \exp\left[-\frac{\left(t - \frac{\sigma_t^2}{\tau} - t_a\right)^2}{2\sigma_t^2}\right] dt_a \tag{8}$$

Substitution of $x = (t - \sigma_t^2/\tau - t_a)/[(2)^{1/2}\,\sigma_t]$ and $dx = -[1/(2)^{1/2}\,\sigma_t]dt_a$ into eqn. 8 results in

$$C(t) = -\frac{C_0}{(\pi)^{1/2}} \exp\left[-\frac{(t - t_R)}{\tau}\right] \exp\left(\frac{\sigma_t^2}{2\tau^2}\right) \int_{(t-\sigma_t^2/\tau - t_a)/(2)^{1/2}\sigma_t}^{-\infty} \exp(-x^2)dx \tag{9}$$

This integral cannot be solved precisely and the error function [erf(y)] must be utilized in the final result. The indefinite integral of the form

$$\mathrm{erf}(y) = \frac{2}{(\pi)^{1/2}} \int_0^y \exp(-x^2)dx \tag{10}$$

when substituted into eqn. 9, yields the final concentration expression for the convolution of an exponential input function with a Gaussian operator.

$$C(t) = \frac{C_0}{2} \exp\left[-\frac{(t - t_R)}{\tau}\right] \exp\left(\frac{\sigma_t^2}{2\tau^2}\right) \left[1 + \mathrm{erf}\frac{\left(t - \frac{\sigma_t^2}{\tau} - t_R\right)}{(2)^{1/2}\sigma_t}\right] \tag{11}$$

However, the concentration profile as a function of distance [$C(z)$], rather than time, is necessary for the calculation of the axial concentration gradient and thus the refractive index gradient in the flow cell. This conversion from time (t) to distance (z) is easily accomplished by noting for constant linear velocity (u) conditions, the time is given by $t = z/u$ and the time variance for a non-retained solute is given by $\sigma_t^2 = \sigma_L^2/u^2$. This results in a final concentration profile as a function of distance of

$$C(z) = \frac{C_0}{2} \exp\left[-\frac{(z - z_R)}{u\tau}\right] \exp\left(\frac{\sigma_L^2}{2u^2\tau^2}\right) \left[1 + \mathrm{erf}\frac{\left(z - \frac{\sigma_L^2}{u\tau} - z_R\right)}{(2)^{1/2}\sigma_L}\right] \tag{12}$$

where σ_L^2 is the length variance contributed by the column or connecting tubing and z_R is the retention distance, analogous to the retention time. Since the functions within the original convolution integral in eqn. 2 are commutative, the final concentration profile (eqns. 11 and 12) is the same regardless of where the exponential broadening occurs. Thus, the same final concentration expression results whether the exponential input arises from a non-ideal injection, a mixing volume, or a detector time constant.

Rectangular input function

A rectangular injection of duration time τ may be described by the following input concentration profile.

$$C(t_a) = C_0 \quad \text{for} \quad t_R \leqslant t_a \leqslant t_R + \tau \tag{13}$$

Convolution of this rectangular injection function with a Gaussian operator is accomplished by substitution into eqn. 2 with the following result:

$$C(t) = \frac{C_0}{(2\pi)^{1/2}\sigma_t} \int_{t_R}^{t_R+\tau} \exp\left[-\frac{(t-t_a)^2}{2\sigma_t^2}\right] dt_a \tag{14}$$

Evaluation of this integral utilizing the error function (eqn. 10) yields the final expression for the concentration profile arriving at the detector:

$$C(t) = \frac{C_0}{2}\left\{\text{erf}\left[\frac{t-t_R}{(2)^{1/2}\sigma_t}\right] - \text{erf}\left[\frac{t-t_R-\tau}{(2)^{1/2}\sigma_t}\right]\right\} \tag{15}$$

Again this expression can be converted to distance units, resulting in a concentration profile as a function of distance:

$$C(z) = \frac{C_0}{2}\left\{\text{erf}\left[\frac{z-z_R}{(2)^{1/2}\sigma_L}\right] - \text{erf}\left[\frac{z-z_R-u\tau}{(2)^{1/2}\sigma_L}\right]\right\} \tag{16}$$

In the limit of small injection time τ, the rectangular injection yields a δ function input and thus a final concentration profile that is purely Gaussian in form.

Stepwise input function

For a gradient program employing a sequence of m steps, of equal duration τ, the input concentration profile can be described by

$$C(t_a) = \sum_{n=1}^{m} \frac{C_0}{m} \quad \text{for} \quad t_R + (n-1)\tau \leqslant t_a \leqslant t_R + m\tau \tag{17}$$

where n is the step number and C_0 is the final concentration of the strong solvent. The stepwise input function is then convolved with a Gaussian operator utilizing eqn. 2, resulting in

$$C(t) = \frac{1}{(2\pi)^{1/2}\sigma_t} \sum_{n=1}^{m} \frac{C_0}{m} \int_{t_R+(n-1)\tau}^{t_R+m\tau} \exp\left[-\frac{(t-t_a)^2}{2\sigma_t^2}\right] dt_a \tag{18}$$

This function is evaluated utilizing eqn. 10 to yield the final concentration profile as a function of time.

$$C(t) = \frac{C_0}{2m} \sum_{n=1}^{m} \left\{\text{erf}\left[\frac{t-t_R-(n-1)\tau}{(2)^{1/2}\sigma_t}\right] - \text{erf}\left[\frac{t-t_R-m\tau}{(2)^{1/2}\sigma_t}\right]\right\} \tag{19}$$

Conversion to distance units results in the final concentration profile for the stepwise input function.

$$C(z) = \frac{C_0}{2m} \sum_{n=1}^{m} \left\{\text{erf}\left[\frac{z-z_R-(n-1)u\tau}{(2)^{1/2}\sigma_L}\right] - \text{erf}\left[\frac{z-z_R-mu\tau}{(2)^{1/2}\sigma_L}\right]\right\} \tag{20}$$

Although this expression for the final axial profile contains equal concentration increments (C_0/m) and a constant step length ($u\tau$), by judicious choice of input functions a variable step height or length may be incorporated.

Linear input function

The input concentration profile for a linear solvent program of duration τ, may be described as follows:

$$C(t_a) = \frac{C_0(t_a-t_R)}{\tau} \qquad \text{for} \qquad t_R \leqslant t_a \leqslant t_R + \tau \tag{21}$$

Convolution of the linear input function is accomplished by substituting eqn. 21 into eqn. 2, resulting in the following form:

$$C(t) = \frac{C_0}{(2\pi)^{1/2}\sigma_t\tau} \int_{t_R}^{t_R+\tau} (t_a - t_R) \exp\left[-\frac{(t-t_a)^2}{2\sigma_t^2}\right] dt_a \tag{22}$$

Integration of eqn. 22 is facilitated by noting that $x \exp(-x^2)$ is a function of the derivative of $\exp(-x^2)$. Thus, the final concentration profile from the convolution of a linear ramp with a Gaussian function is

$$C(t) = \frac{C_0\sigma_t}{(2\pi)^{1/2}\tau} \left\{\exp\left[-\frac{(t-t_R)^2}{2\sigma_t^2}\right] - \exp\left[-\frac{(t-t_R-\tau)^2}{2\sigma_t^2}\right]\right\} - \frac{C_0(t_R-t)}{2\tau} \left\{\text{erf}\left[\frac{(t-t_R)}{(2)^{1/2}\sigma_t}\right] - \text{erf}\left[\frac{(t-t_R-\tau)}{(2)^{1/2}\sigma_t}\right]\right\} \tag{23}$$

Again, converting to distance units yields the axial concentration profile

$$C(z) = \frac{C_0\sigma_L}{(2\pi)^{1/2}u\tau}\left\{\exp\left[-\frac{(z-z_R)^2}{2\sigma_L^2}\right] - \exp\left[-\frac{(z-z_R-u\tau)^2}{2\sigma_L^2}\right]\right\} - \frac{C_0(z-z_R)}{2u\tau}\left\{\mathrm{erf}\left[\frac{z-z_R}{(2)^{1/2}\sigma_L}\right] - \mathrm{erf}\left[\frac{z-z_R-u\tau}{(2)^{1/2}\sigma_L}\right]\right\} \quad (24)$$

as a function of the length standard deviation (σ_L) and the linear velocity (u).

ACKNOWLEDGEMENTS

We gratefully acknowledge the kind gift of high-purity solvents from the Burdick and Jackson Division of Baxter Healthcare Corp. We also wish to thank Dr. M. D. Morris (University of Michigan) and Dr. T. A. Nevius (The Anspec Co.) for helpful discussions, and Dr. S. R. Crouch (Michigan State University) for his thoughtful and critical evaluation of this work.

REFERENCES

1 L. R. Snyder and J. J. Kirkland, *Introduction to Liquid Chromatography*, Wiley, New York, 1979, p. 133.
2 D. Betteridge, E. L. Dagless, B. Fields and N. F. Graves, *Analyst (London)*, 103 (1978) 897.
3 D. O. Hancock and R. E. Synovec, *Anal. Chem.*, 60 (1988) 1915.
4 J. E. Stewart, *Appl. Opt.*, 20 (1981) 654.
5 J. E. Stewart, *Anal. Chem.*, 53 (1981) 1125.
6 C. F. deMay and C. C. Helms, *U.S. Pat.*, 4 192 614 (1980).
7 J. N. Little and G. J. Fallick, *J. Chromatogr.*, 112 (1975) 389.
8 D. J. Bornhop, T. G. Nolan and N. J. Dovichi, *J. Chromatogr.*, 384 (1987) 181.
9 J. Pawliszyn, *Anal. Chem.*, 58 (1986) 243.
10 J. Pawliszyn, *Anal. Chem.*, 58 (1986) 3207.
11 C. E. Evans and V. L. McGuffin, *J. Chromatogr.*, 459 (1988) 119.
12 J. D. Ingle and S. R. Crouch, *Spectrochemical Analysis*, Prentice-Hall, Englewood Cliffs, NJ, 1988, p. 373.
13 F. A. Jenkins and H. E. White, *Fundamentals of Optics*, McGraw-Hill, New York, 1976, pp. 115–126.
14 S. M. McCown, D. Southern, B. E. Morrison and D. Gartiez, *J. Chromatogr.*, 352 (1986) 465.
15 E. D. Katz, C. H. Lochmuller and R. P. W. Scott, *Anal. Chem.*, 61 (1989) 349.
16 K. Peck and M. D. Morris, *J. Chromatogr.*, 448 (1988) 193.
17 G. Taylor, *Proc. R. Soc. London, Ser. A*, 219 (1953) 186.
18 J. J. van Deemter, F. J. Zuiderweg and A. Klinkenberg, *Chem. Eng. Sci.*, 5 (1956) 271.
19 J. H. Knox, *J. Chromatogr. Sci.*, 15 (1977) 352.
20 M. J. E. Golay, in D. H. Desty (Editor), *Gas Chromatography 1958*, Academic Press, New York, 1958, pp. 36–55.
21 R. Aris, *Proc. R. Soc. London, Ser. A*, 235 (1956) 67.
22 C. N. Reilley, G. P. Hildebrand and J. W. Ashley, Jr., *Anal. Chem.*, 34 (1962) 1198.
23 J. C. Sternberg, *Adv. Chromatogr.*, 2 (1966) 205.
24 E. W. Marchand, *Gradient Index Optics*, Academic Press, New York, 1978, pp. 3–6.
25 C. R. Wilke and P. Chang, *AIChE J.*, 1 (1955) 264.
26 R. M. McCormick and B. L. Karger, *Anal. Chem.*, 52 (1980) 2249.
27 S. Levin and E. Grushka, *Anal. Chem.*, 59 (1987) 1157.